



ACADÉMIE
DES SCIENCES
INSTITUT DE FRANCE

Comptes Rendus

Physique

Leo Cerfolli, Jean-Francois Ripoll, Richard Bertram Horne, Alexandra Michelle Wold and Robert Andrew Marshall

Ray tracing of very low frequency waves produced by active experiments or lightning events at low Earth orbit

Volume 26 (2025), p. 285-294

Online since: 18 March 2025

<https://doi.org/10.5802/crphys.238>

 This article is licensed under the
CREATIVE COMMONS ATTRIBUTION 4.0 INTERNATIONAL LICENSE.
<http://creativecommons.org/licenses/by/4.0/>



*The Comptes Rendus. Physique are a member of the
Mersenne Center for open scientific publishing*
www.centre-mersenne.org — e-ISSN : 1878-1535



Research article / *Article de recherche*

Ray tracing of very low frequency waves produced by active experiments or lightning events at low Earth orbit

Lancer de rayons d'ondes à très basse fréquence produites par des expériences actives ou des éclairs à orbite terrestre basse

Leo Cerfolli^{Ⓜ, a, b}, Jean-Francois Ripoll^{Ⓜ, *, a, b}, Richard Bertram Horne^{Ⓜ, c},
Alexandra Michelle Wold^{Ⓜ, d} and Robert Andrew Marshall^{Ⓜ, d}

^a CEA, DAM, DIF, F-91297, Arpajon, France

^b UPS, CEA, LMCE, 91297 Bruyères-le-Châtel, France

^c British Antarctic Survey, Natural Environment Research Council, Cambridge, UK

^d Ann & H.J. Smead Department of Aerospace Engineering Sciences, University of Colorado Boulder, CO, USA

E-mails: leo.cerfolli@cea.fr (L. Cerfolli), jean-francois.ripoll@cea.fr (J.-F. Ripoll),
rh@bas.ac.uk (R. B. Horne), alexandra.wold@colorado.edu (A. M. Wold),
robert.marshall@colorado.edu (R. A. Marshall)

Abstract. We investigate the propagation in the plasmasphere of Very Low Frequency (VLF) electromagnetic waves, such as natural lightning-generated whistler waves and waves produced by active experiments. An active experiment is an artificial controlled disturbance of the low orbit space or the ionosphere. The aim is often to produce electromagnetic waves for removing high-energy particles (mostly electrons). We study the wave propagation parameters whether they are geometric, background, or intrinsic parameters, such as the magnetic field model, the ambient plasma density model of the plasmasphere, and the wave frequency. All of these parameters cause different behaviors of propagation, which are discussed in this article.

Résumé. Nous explorons la propagation d'ondes électromagnétiques de très basses fréquences dans la plasmasphère, telle que des ondes de type siffleur générées par les éclairs ou des ondes produites par des expériences actives. Une expérience active est une perturbation artificielle et contrôlée de l'espace proche de la Terre ou de l'ionosphère souvent dans l'idée de dépeupler cette région de particules de hautes énergies (souvent des électrons). Pour le faire, nous ordonnons les paramètres de propagation selon trois classes : les paramètres de fond, les paramètres géométriques et les paramètres intrinsèques. Les paramètres de fond regroupent le modèle de champ magnétique ainsi que celui de la densité plasmasphérique. Ils influent via leurs valeurs aux différents points de calcul ainsi que leurs gradients. Le paramètre intrinsèque ici établi est la fréquence de l'onde. Avec ces paramètres nous verrons que des comportements très différents sont accessibles.

Keywords. Ray tracing, Very low frequency waves, Magnetic field models, Low Earth orbit.

Mots-clés. Ray-tracing, Ondes très basses fréquences, Modèles de champs géomagnétiques, Basses orbites.

* Corresponding author

Funding. Direction Générale de l'Armement (DGA), Agence pour l'Innovation de Défense (AID).

Manuscript received 13 September 2024, revised 15 November 2024 and 20 January 2025, accepted 4 February 2025.

1. Introduction

The plasmasphere, named by [1], is the toroidal region of cold electrons (1–5 eV) located between the ionosphere from ~90 km of altitude up to ~1000 km [2] and its external limit, the plasmopause. The plasmopause is generally defined as the location where the electron density decreases by a factor 5 on a radial distance of ~3000 km [3]. The plasmopause generally locates at the 100 #/cc density level [4]. Many types of electromagnetic waves propagate within the plasmasphere and we focus in this article only on very low frequency (VLF) waves as natural lightning-generated whistler (LGW) waves as well as waves produced by active experiments. An active experiment is an artificial controlled disturbance in the low orbit space or in the ionosphere. The aim is often to produce waves for removing high-energy particles (mostly electrons) forming radiation belts [5], which are source of hard radiations for orbiting satellites. As instances of active experiments, the most noticeable are Barium releases as CRRES-1991 [6] and more recently the amplification of local waves by the rocket exhausts of hydrazine burn [7]. Here, we study the propagation of VLF waves through a parametric numerical study involving the HOTRAY code [8], varying various parameters such as the magnetic field model, the ambient plasma density model of the plasmasphere, and the wave frequency.

In Section 2, we briefly describe the numerical method and code for wave propagation computation. Section 3 shows the importance of the magnetic field model through model comparisons. Section 4 is dedicated to the description and role of the diffusive equilibrium model driving the electron density in the Earth's plasmasphere. Section 5 shows the influence of the wave frequency for wave propagation. Conclusions are gathered in the last section.

2. Simulation of wave propagation

We use the HOTRAY code [8] to simulate VLF waves. The HOTRAY code uses the eikonal approximation of geometric optics to simulate the curved propagation and find the ray path ([8] and references in there). Based on Eikonal approximation, the main resolved equations are given by:

$$\frac{\partial \vec{R}}{\partial t} = -\frac{\partial D / \partial \vec{k}}{\partial D / \partial \omega} = \vec{v}_g \quad (1)$$

$$\frac{\partial \vec{k}}{\partial t} = \frac{\partial D / \partial \vec{R}}{\partial D / \partial \omega} \quad (2)$$

Equation (1) solves the propagation in space, where R is the position vector, t the time, D the dispersion term and k the complex wave vector. HOTRAY assumes that the ambient plasma is non-relativistic and that wave amplitudes are small for applying both the linear theory and linear instability growth and damping. The code works with the underlying WKB (Wentzel–Kramers–Brillouin), $|1/k(dk/dx)| \ll k$, which means that the change of wavelength over a wavelength should be small [9]. This approximation fails when $k \rightarrow 0$ or when $dk/dx \rightarrow \infty$, or whenever the wave approaches either a cutoff or a resonance. This implies the spatial gradients in the ambient cold plasma are assumed to be small compared with the wavelength. From a numerical point of view, the WKB approximation is generally satisfied, as we define the inhomogeneous plasma by a succession of straight propagation into layers of homogeneous plasma where density and magnetic field are constant (see below the case of magneto-reflection).

In HOTRAY, the chosen strategy is to launch given frequency waves so the frequency of the wave, $f_0 = \omega_0/2\pi$, or its pulsation ω_0 , is always fixed. For computing the amplification/damping, since we fix the pulsation real, the complex contribution given by the relation dispersion comes from the wave vector (see exception below for magnetoreflexion). In Equation (1) the right-hand side can be identified as the wave group velocity. Equation (2) solves for the evolution of the wave vector according to the dispersion relation. In all points along the ray path, we have to solve the full dispersion relation, given by

$$D(\vec{R}, \vec{k}, \omega) = 0. \quad (3)$$

The complete expression of the dispersion relation is given in [8]. Equation (3) can be written as $An^4 + Bn^2 + C = 0$.

Furthermore, the numerator in the right-hand side of Equation (2) can be developed as

$$\frac{\partial D}{\partial \vec{R}} = \frac{\partial D}{\partial \vec{B}} \frac{\partial \vec{B}}{\partial \vec{R}} + \frac{\partial D}{\partial N} \frac{\partial N}{\partial \vec{R}} + \frac{\partial D}{\partial \vec{k}} \frac{\partial \vec{k}}{\partial \vec{R}} \quad (4)$$

The three terms in the right-hand side of Equation (4) highlight the competition between magnetic field gradients, density gradients, and variations of the wave vector. In the third term, dk/dR , the variations in position of the wave vector account for changes in amplitude and the orientation and norm of the wave vector.

The fact that the wave vector is complex implies the wave amplitude can be damped or amplified. The wave vector direction is defined by two angles: the wave normal angle defined as the angle between the wave vector and the local magnetic field and the azimuthal angle defined as the geographic eastward component of the wave vector.

Background parameters regrouping the magnetic field and the density model appear as gradients in Equation (4) as well as single-point values in the dispersion relation. An important condition for wave propagation is dictated by the lower hybrid (LH) frequency. The LH frequency is the limit for allowing the bounce of the ray at high latitude (see more below). Its definition is given by:

$$\omega_{\text{LH}} = \left[(\Omega_i \Omega_e)^{-1} + \omega_{pi}^{-2} \right]^{-1/2} \quad (5)$$

where $\Omega_i = q_i B / m_i$ is the cyclotron pulsation, q_i is the charge, m_i is the mass, e and i indices refer to electrons and ions respectively, and ω_p is the plasma pulsation. ω_{LH} The lower hybrid frequency varies as B , through both the cyclotron pulsation terms, and as the square root of the electron density. An increase in B or in $\sqrt{n_e}$ increases the lower hybrid frequency. This shows another competition between the magnetic field and the plasma density for each single location of the wave during its propagation.

Landau resonant interactions are included in the code and occur when the electron speed is near the phase velocity of the wave. This creates an energetic flux between the wave and the electron. If the wave gives energy to the electron, then the wave is damped. Otherwise, the wave is amplified. The spatial scale for the Landau instability growth rate is dictated by each cell size and the local growth rate, Γ_i , is driven by the imaginary part of the local wave vector k_i in the layer number i by $\Gamma_i(k) = \Im(k_i) \Delta r_i$, where \Im is the imaginary operator and r_i the spatial step. Expanding the dispersion relation in Taylor series for $\gamma/\omega \ll 1$, [10] show that $\Im(k_i) = -(\gamma_i) / ((\partial D / \partial k) / (\partial D / \partial \omega)_i)$ where the denominator can be identified as the group velocity in cell i . Near a magnetoreflexion, the parallel group velocity changes sign, passing to zero, while the perpendicular group velocity, thus the group velocity, does not go to zero—otherwise the wave would not continue to propagate.

Near zero parallel group velocity can bring numerical errors because the spatial step becomes numerically too small. In order to avoid these errors, the growth rate, $\Gamma_i(k)$, is rather computed in the time domain. In that case, the numerical method is to assume the pulsation is not real anymore but switch to a complex number written as $\omega_i = \omega_0 + j\gamma_i$, with j the imaginary unit,

Table 1. Species and plasma parameters used in this study. The drift velocity is always zero.

Species index	Species	Thermal velocity perpendicular to B (keV)	Parallel thermal velocity (keV)	Density (#/m ⁻³)
1	O ⁺	10 ⁻⁴	10 ⁻⁴	10 ⁹
2	e ⁻	10 ⁻³	10 ⁻³	10 ¹⁰
3	He ⁺	10 ⁻⁴	10 ⁻⁴	10 ⁹
4	H ⁺	10 ⁻⁴	10 ⁻⁴	8 × 10 ⁹
5	H ⁺	10 ⁻⁴	10 ⁻⁴	2.782 × 10 ⁷
6	e ⁻	2.5 × 10 ⁻²	2.5 × 10 ⁻²	2.5 × 10 ⁷
7	e ⁻	1.5 × 10 ⁻¹	1.5 × 10 ⁻¹	2.5 × 10 ⁶
8	e ⁻	1	1	2.5 × 10 ⁵
9	e ⁻	5	5	5 × 10 ⁴
10	e ⁻	20	20	2 × 10 ⁴

γ_i the imaginary part of the pulsation leading to a local growth rate, $\Gamma_i = \gamma_i \Delta t_i$, and $\omega_0 = 2\pi f_0$ [8]. The complex pulsation then serves to compute the damping/growth of the wave amplitude but the wave frequency is still maintained constant at f_0 . The reflection point is neither a cut-off where k tends to zero nor a resonance where k becomes very large. k rather remains finite. However, near magneto-reflection (with the parallel group velocity passing to zero) the WKB modeling fails in principle but still gives an approximation accurate enough to describe the wave propagation at the turning point for the propagation of a low frequency wave in the Earth's magnetosphere (e.g. [11]).

There are three available thermal ions causing Landau resonance, often physically leading to Landau damping. They correspond to the common species in the plasmasphere, namely H⁺, He⁺, O⁺. Their density, N_b , and proportions are adjusted following [12] such that their presence adds a warm plasma correction to the cold electron background. The proportions used here is given in Table 1 and are the same as in [12]. Distribution functions are given by

$$f_i = \frac{1}{\pi^{3/2} \alpha_{\perp i}^2 \alpha_{\parallel i}} e^{-((v_z - v_{di})^2 / \alpha_{\parallel i}^2)} \left[\Delta_i e^{-(v_{\perp}^2 / \alpha_{\perp i}^2)} + \frac{1 - \Delta_i}{1 - \beta_i} \left(e^{-(v_{\perp}^2 / \alpha_{\perp i}^2)} - e^{-(v_{\perp}^2 / \beta_i \alpha_{\perp i}^2)} \right) \right]$$

where i refers to the specie, Δ determines the depth of the loss cone, v_d is the drift velocity along the magnetic field line, α_{\perp} or α_{\parallel} is the thermal velocity perpendicular/parallel to the magnetic field given in keV using $1/2 m_i \alpha^2$, and β measures the width of the loss cone. Here, we assume there is no loss cone ($\Delta = 1$) and the drift velocity along the magnetic field line is 0. Then the distribution function reduces as

$$f_i = \frac{1}{\pi^{3/2} \alpha_{\perp i}^2 \alpha_{\parallel i}} e^{-(v_z^2 / \alpha_{\parallel i}^2)} e^{-(v_{\perp}^2 / \alpha_{\perp i}^2)}$$

In our simulations, we choose both the perpendicular and parallel thermal velocities so that they are equals.

3. Influence of the magnetic field model

Active experiments are generally performed at low Earth orbit (from 100 km to 1500 km) and produce electromagnetic waves in a large range of L-shells according to the experiment's altitude and latitude. The L-shell is the Earth's radius normalized distance of a given field line at the magnetic equator. The L-shell discriminates the field lines and depends on the chosen magnetic field model. At low Earth orbit (LEO), there are three main models for Earth's magnetic field: the pure dipole used by many codes for simplicity, as HOTRAY, the eccentric tilted dipole, which is the

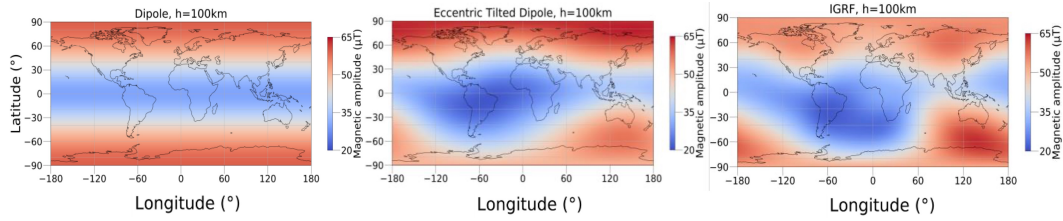


Figure 1. Magnetic field amplitude projected on Earth at 100 km for (left) a pure dipole field model as used in HOTRAY, (center) an eccentric tilted dipole field model, and (right) the IGRF 13th generation model.

most accurate dipolar approach of the Earth’s magnetic field, and the full International Geomagnetic Reference Field (IGRF) model. Dipolar models have orthogonal metrics in classic space coordinates (like geographic or magnetic coordinates) which provide mathematical simplifications. The eccentric tilted dipole is a pure dipole for which the main axis is not the Earth’s rotation axis, since it is tilted, and the magnetic center does not correspond to the geographic center, since it is shifted. The IGRF is defined by a potential as a harmonic development around a tilted dipole field and is based on a potential defined from ground measurements. The potential expression is:

$$V(r, \theta, \varphi, t) = R_e \sum_{n=1}^N R^{n+1} [g_n^m \cos(m\varphi) + h_n^m \sin(m\varphi)] P_n^m(\cos(\theta)) \quad (6)$$

where coefficients noted h and g are established from ground measurements, R_e is the Earth’s radius, $R = R_e/r$, r is the radial distance, θ is the latitude, φ is the longitude and P_n^m are associated Legendre polynomials.

The magnetic field is then derived from the potential as

$$\vec{B} = -\vec{\nabla}(V) \quad (7)$$

We use the 13th generation of the IGRF coefficients [13]. In Figure 1, we plot the magnetic amplitude with respect to latitude and longitude at 100 km of altitude. This altitude is chosen, since it is the commonly adopted limit for electron precipitations in the upper atmosphere. Both the eccentric tilted dipole model and the IGRF model have the same main structures. First, the “S shape” is the global shape along longitude produced by the variation of the magnetic equator along longitude. The second is the South Atlantic Anomaly (SAA), which is a zone of large depression in magnetic amplitude. The center of this depression is different between the eccentric tilted dipole and the IGRF models. For the eccentric tilted dipole, the center is at -30° of latitude and -10° of longitude, while, for IGRF it is centered at -40° of latitude and between -60° and -30° of longitude. This depression is a consequence of both the tilted axis and the shift of the magnetic center. The global shape of the SAA is also different for the two models. In the IGRF model, high order harmonics ($n \geq 3$ in Equation (5)) constrain the SAA to fit with ground measurements.

In Figure 2, we plot the relative error between the two dipolar models and the IGRF. Differences for each comparison are located around the IGRF SAA. The relative error reaches a maximum of 101% for the dipole and 53% for the eccentric tilted dipole. Elsewhere, dipolar models are rather accurate. However, the relative error does not show topologic differences seen on the field lines (not discussed here). Field lines end up different for each model, with implication on the propagation as field lines act as a wave guide. Note that, for very low frequency waves, the plasmopause also acts as a wave guide [14]. The consequence is that ray paths can change. In the following sections, the HOTRAY code will be used with the dipole field in order to provide first results for future comparisons with the IGRF model, currently being integrated in HOTRAY.

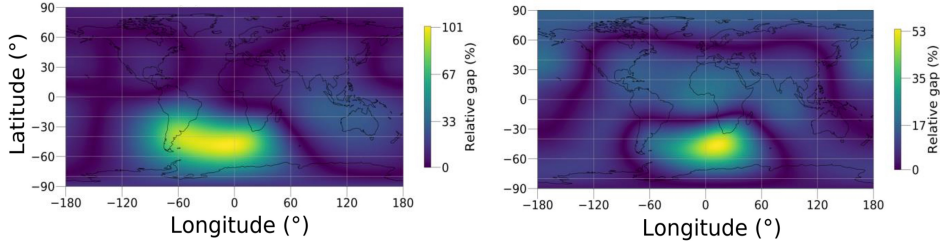


Figure 2. Magnetic field amplitude relative error at 100 km, (left) for a pure dipole field model compared with the IGRF model and (right) for an eccentric tilted dipole field model compared with the IGRF model. Most of the errors are concentrated in the SAA region.

4. Influence of the plasmaspheric density model

The HOTRAY code computes ray-path evolving in an ambient medium filled of cold ions and electrons. Their density is given by the diffusive equilibrium model, which equates the electron density with the ionic densities $N_e = N_i$. The diffusive equilibrium further decomposes N_i in:

$$N_i(R) = N_b N_{de}(R) N_{li}(R) N_{pl}(R) \quad (8)$$

where the density N_b is the number of particles (#) per meter cube on a given point of reference at an altitude R_b . N_b is a scale density which scales the density profile, defined at all radii, R , of the whole plasmasphere and will be studied below. The dimensionless density N_{de} is the profile of diffusive equilibrium along the radial direction, which depends on temperature T_{DE} , and gravity, $g(R_b)$, for each plasma component, as follows

$$N_{de}(R)^2 = \sum_{i=1}^n \eta_i \exp\left(-\frac{G}{H_i}\right) \quad (9)$$

with

$$H_i = \frac{k_B T_{DE}}{M_i m_p g(R_b)} \quad (10)$$

In Equations (9)–(10) giving the profile of the diffuse equilibrium, each exponential term is weighted by the proportion of the plasma component ions, η_i , which is a function of the radial distance. There are three available species: H^+ , He^+ , and O^+ . This highlights the importance of the characteristic length of thermal diffusion, H_i , prescribed for each component of the ambient plasma. The associated thermal velocity is given by $v_{th} \approx \sqrt{3k_B T_{DE}/m}$. G is the geopotential height, k_B is the Boltzmann constant, M_i is the mass number for the ion labeled i , and m_p the proton mass.

The dimensionless density N_{li} connects with the bottom of the ionosphere through a decreasing exponential function defined from the chosen altitude of the bottom ionosphere R_0 (in km), up to its height H (in km) as follows

$$N_{li} = 1 - \exp\left[-(R - R_0)^2 / H^2\right] \quad (11)$$

The dimensionless density profiler N_{pl} forms the plasmapause by introducing a latitude dependence through the L-shell value, L , and curves the density isolines with the plasmapause shape, at position L_p expressed in L-shell.

$$N_{pl} = \exp^{-\frac{(L-L_p)^2}{H_p^2}} + \left(1 - \exp^{-\frac{(L-L_p)^2}{H_p^2}}\right) \left(\frac{R_c}{R}\right)^a + \left(1 - \left(\frac{R_c}{R}\right)^a\right) \left(\exp^{-\frac{(R-R_c)^2}{H_s^2}}\right) \quad (12)$$

H_p is the half width of the plasmapause boundary in L value. R_c is the geocentric distance in km to the level at which the density outside the plasmapause field line is equal to the density inside.

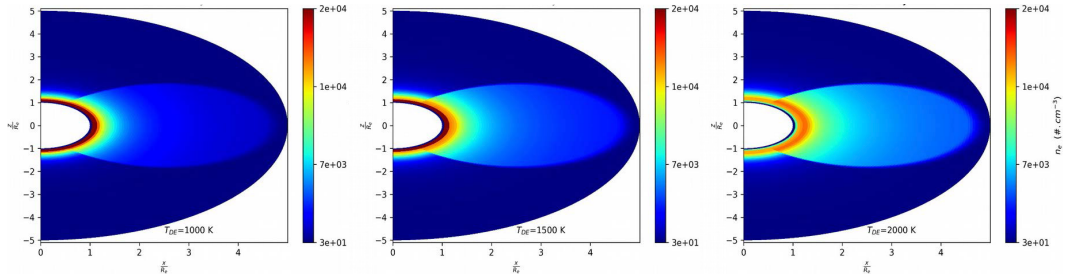


Figure 3. Variation of the diffusive equilibrium electron density with temperature for (left) 1000 K, (center) 1500 K, and (right) 2000 K.

H_s is the scale height of radial density decrease. Finally, a determines how the density falls off outside the plasmopause.

The following subsections are dedicated to the influence of the diffusive equilibrium temperature, directly influencing the diffusion of the electron density from Earth's atmosphere and the absolute value of the electron density in HOTRAY simulations of VLF waves.

4.1. Influence of the diffusive equilibrium temperature

For each component, the characteristic length of thermal diffusion is proportional to the ratio of temperature with gravity so that, for a given position, as gravity is fixed, the scale length becomes directly proportional to temperature. In Figure 3, we vary the diffusive equilibrium temperature from $T = 1000$ to 2000 K and show the variation of the electron density. For these simulations, the scale density is fixed at $n_e = 2.7 \times 10^9 \text{ m}^{-3}$ and the plasmopause at $L_p = 4.5$. The temperature radially diffuses density at higher radial distance and follows the plasmopause. The diffusive scale length increases with temperature so that, as the temperature increases, more plasma components can reach higher altitudes driven by their thermal velocity.

Figure 4 shows four rays launched at a latitude of -40° and 400 km of altitude into the plasmasphere computed using the diffusive equilibrium at temperatures varying from 1000 to 4000 K. For all rays, we find the ray path is the same, except that it is shortened as the temperature increases. This is due to the shape of density isolines, which remains the same while the value of the isodensity is different according to the temperature. The more the density value is large, the more matter the wave passes through, which causes the waves to be more damped by the Landau damping effect. Thus, as the temperature increases, waves vanish earlier on the ray path.

4.2. Influence of the density scaling

In Equation (8) the density parameter, N_b , scales all values of density in the plasmasphere leading to different behaviors for a given wave. In Figure 5, we propagate a 5 kHz whistler wave for different values of N_b . For low density, the magnetic field dominates the propagation, allowing the wave to reach the atmosphere on the conjugate point of the launch location and to vanish in the upper atmosphere without bouncing (e.g. red line in Figure 5). The magnetic field acts as a wave guide for the propagation. At high latitude, when density is high enough compared with the magnetic field, the lower hybrid frequency can exceed the wave frequency and permits the lower hybrid resonance to occur. In that case, the wave resonance cone is reduced to zero as the surface of refractive index becomes closed. A normal propagation, i.e. a perpendicular propagation to the local magnetic field, is thus theoretically allowed so that the wave's normal angle can reach 90° .

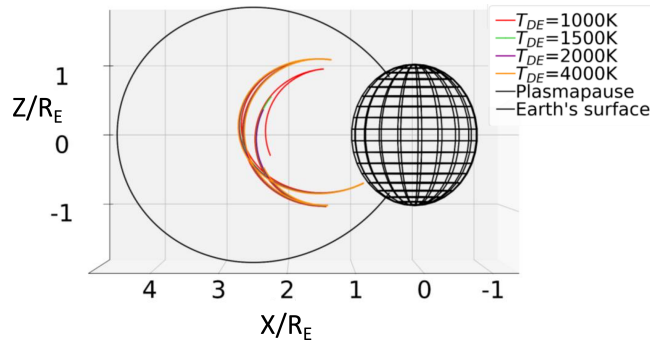


Figure 4. Ray paths of a 5 kHz whistler wave for different temperatures, from $T = 1000$ to 4000 K. The ray path is the same but shortens as the temperature increases.

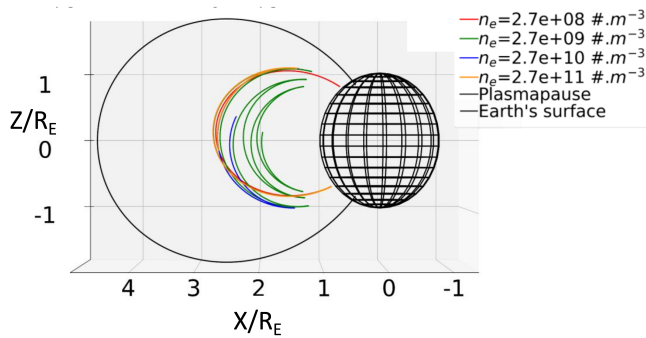


Figure 5. Ray paths of a 5 kHz whistler wave for different scale density at 2000 K. With higher density at fixed magnetic amplitude magnetorelections are allowed.

As the wave propagates perpendicularly, its wave normal angle will now exceed 90° , so that the wave is reflected back. A bounce has happened. Several of these magnetic bounces can occur in a common propagation. This effect is combined with the previously described effect of the density effect. The more the encountered density is high, the more the wave damping is strong, so that the ray path is shortened along the ray path.

5. Influence of wave parameters: the frequency

Here, we study the importance of the wave frequency within the whistler range, as this parameter influences the escape point from the ionosphere, the bounce at high latitude, and the region reached by the wave. Using an electron temperature of 2000 K and an electron density of $n_e = 2.7 \times 10^9 \text{ m}^{-3}$, we propagate several waves at frequencies ranging from 1 kHz to 15 kHz within the plasmasphere. Results are presented in Figure 6. The 15 kHz ray only follows the field line because the lower hybrid frequency never comes near the wave frequency so that magnetorelections are never allowed and the ray continues to follow the field line. This ray reaches the Earth's surface before its wave normal angle can reach the 90° critical value for allowing propagation in the opposite direction. Lower frequency rays, from 1 to 10 kHz, are conversely able to bounce between the two hemispheres. The lowest frequency waves at 1 and 2 kHz have bounced trajectories that are outward directed, i.e. each mirror point increases in altitude. However, higher frequency waves of 5 and 10 kHz have an inward propagation after the

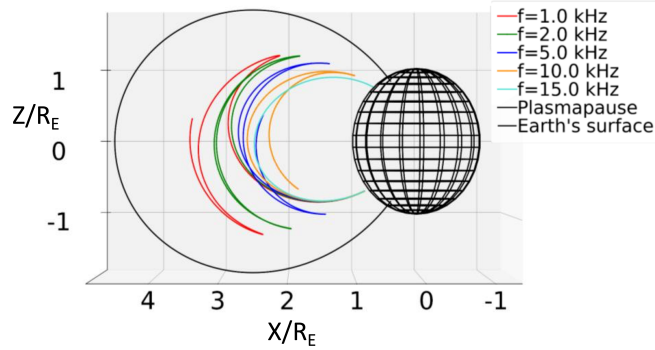


Figure 6. Ray path for several wave frequencies in the whistler range, from 1 kHz to 10 kHz, for an ambient electron plasma at 2000 K. The 15 kHz wave does not bounce, since the lower hybrid frequency is never reached. Inward and outward propagation is allowed according to the frequency values.

first bounce, i.e. each mirror point's altitude successively decreases. This is due to a competition between the magnetic field shape and the density.

6. Conclusions

In this article, we study the main parameters of the propagation of very low frequency waves in the plasmasphere using the British Antarctic Survey (BAS) HOTRAY code. Comparing various magnetic field models, we find that the relative error between a pure dipole field model and the IGRF model reaches a maximum of 101% in the SAA region at 100 km. The relative error reduces to 53% for the eccentric tilted dipole field model. An ongoing task is to implement the IGRF model into HOTRAY. The electron density of the plasmasphere model has two main parameters, the temperature of the diffusive equilibrium and the scale density. The temperature diffuses the density to higher L-shells. We find it does not change the ray path but shortens it as temperature increases due to stronger Landau damping. The scale density defines isodensity lines, which can allow (or not) magnetorelections according to the value of the local lower hybrid frequency. Finally, the frequency determines whether or not the propagating wave bounces. As the bounce is allowed (or not), the propagation remains outward for low-frequency waves (<5 kHz in our simulation). For higher frequencies, the propagation evolves to an earthward propagation as soon as the first bounce has occurred.

Declaration of interests

The authors do not work for, advise, own shares in, or receive funds from any organisation that could benefit from this article, and have declared no affiliation other than their research organisations.

Funding

J-FR and LC thank the Direction Générale de l'Armement (DGA) and the Agence pour l'Innovation de Défense (AID) for funding the ASTRID project "PACTE- ESPACE".

References

- [1] D. L. Carpenter, “Whistler evidence of a ‘knee’ in the magnetospheric ionization density profile”, *J. Geophys. Res.* **68** (1963), no. 6, pp. 1675–1682.
- [2] P.-L. Blelly and D. Alcaydé, “Ionosphere”, in *Handbook of the Solar-Terrestrial Environment* (Y. Kamide and A. Chian, eds.), Springer-Verlag: Berlin, Heidelberg, 2007, pp. 189–220.
- [3] D. L. Carpenter and R. R. Anderson, “An ISEE/whistler model of equatorial electron density in the magnetosphere”, *J. Geophys. Res.* **97** (1992), no. A2, pp. 1097–1108.
- [4] J.-F. Ripoll, S. A. Thaller, D. P. Hartley, et al., “Statistics and empirical models of the plasmasphere boundaries from the Van Allen Probes for radiation belt physics”, *Geophys. Res. Lett.* **49** (2022), article no. e2022GL101402.
- [5] J.-F. Ripoll, S. G. Claudepierre, A. Y. Ukhorskiy, C. Colpitts, X. Li, J. Fennell and C. Crabtree, “Particle dynamics in the earth’s radiation belts: review of current research and open questions”, *J. Geophys. Res. Space Phys.* **125** (2020), article no. e2019JA026735.
- [6] D. Schriver and G. Haerendel, “Stimulated auroral precipitation by wave-particle interactions: Implications for the CRRES satellite mission”, *J. Geophys. Res.* **96** (1991), no. A7, pp. 11403–11419.
- [7] P. A. Bernhardt, W. C. Bougas, M. K. Griffin, et al., “Strong amplification of ELF/VLF signals in space using neutral gas injections from a satellite rocket engine”, *Radio Sci.* **56** (2021), article no. e2020RS007207.
- [8] R. B. Horne, “Path-integrated growth of electrostatic waves: the generation of terrestrial myriametric radiation”, *J. Geophys. Res.* **94** (1989), pp. 8895–8909.
- [9] D. G. Swanson, *Plasma Waves*, 2nd edition, Institute of Physics Publishing: Bristol, Philadelphia, 2003.
- [10] M. Ashour-Abdalla and C. F. Kennel, “Nonconvective and convective electron cyclotron harmonic instabilities”, *J. Geophys. Res.* **83** (1978), no. A4, pp. 1531–1543.
- [11] E. R. Tracy, A. J. Brizard, A. S. Richardson and A. N. Kaufman, *Ray Tracing and Beyond, Phase Space Methods in Plasma Wave Theory*, Cambridge University Press: Cambridge, 2014.
- [12] R. M. Thorne and R. B. Horne, “Landau damping of magnetospherically reflected whistlers”, *J. Geophys. Res.* **99** (1994), no. A9, pp. 17249–17258.
- [13] P. Alken, E. Thébault, C. D. Beggan, et al., “International Geomagnetic Reference Field: the thirteenth generation”, *Earth Planets Space* **73** (2021), article no. 49.
- [14] U. S. Inan and T. F. Bell, “The plasmopause as a VLF wave guide”, *J. Geophys. Res.* **82** (1977), no. 19, pp. 2819–2827.